JOURNAL OF AGRICULTURAL AND FOOD CHEMISTRY

Article

pubs.acs.org/JAFC

Food-Grade Submicrometer Particles from Salts Prepared Using Ethanol-in-Oil Mixtures

Jerome P. Paques,[†,‡] Erik van der Linden,[‡] Leonard M.C. Sagis,*[,‡] and Cees J. M. van Rijn[†]

[†]Laboratory of Organic Chemistry, Wageningen University, Dreijenplein 8, 6703 HB Wageningen, The Netherlands

[‡]Physics and Physical Chemistry of Foods, Wageningen University, Bomenweg 2, 6703 HD Wageningen, The Netherlands

ABSTRACT: A simple method for preparing food-grade particles in the submicrometer range of ethanol soluble salts using ethanol-in-oil (E/O) mixtures is described. Salts $CaCl_2 \cdot 2H_2O$ and $MgCl_2 \cdot 6H_2O$ were dissolved in ethanol that subsequently was mixed with a medium-chain triglyceride oil phase. It was found that type and concentration of salt have a significant influence on the miscibility of ethanol and oil phase and on the stability of E/O mixtures. The ethanol phase was evaporated from the mixture at elevated temperatures, and salt particles with dimensions in the submicrometer range (6−400 nm) remained suspended in the oil phase. It was found that the concentration of salt and volume fraction of ethanol in MCT oil have a significant influence on the size distribution of salt particles. The size of $CaCl_2$ and $MgCl_2$ submicrometer particles was ascertained by scanning electron microscopy and dynamic light scattering.

KEYWORDS: *calcium chloride, magnesium chloride, submicrometer particles, ethanol-in-oil mixtures*

INTRODUCTION

Submicrometer particles have a wide range of applications. They can be used in medical applications,[1−3] for analytics,[4,5] in cosmetics,[6,7] in food products,[8−10] as templates,[11−13] or in optical and electronic applications.[14−19]

Submicrometer particles can find application in cases where microparticles cannot be used. For instance, membranes developed for emulsification can have very small pores and submicrometer particles of salts could pass through these pores, whereas microparticles (5−20 μm) would block them. Also, much research has been done with glass microchannels[20−28] where different reactions occur within the small channels when substances are mixed (for example, alginate gelation[28]). Such submicrometer salt particles could be ideal in this application since they will not block the channels and they allow development of even narrower channels. Chemical reactions and dissolution of the submicrometer salt particles can occur faster as well compared to microparticles, which have a smaller surface to volume ratio.

Submicrometer salt particles dispersed in oil may be used for alginate gelation. Tong et al. describe a method for formation of colloidosomes (430 μm) with alginate gel cores and shells of porous $CaCO_3$ microparticles.[29]

Fortification of foods and beverages with mineral salts, such as calcium and magnesium, is an increasingly common practice.[30−39] Addition of salts in a solubilized state can have disadvantages. Emulsion stability can be influenced by $CaCl_2$, which promotes droplet flocculation.[40,41] Salts can influence enzyme activity and react with other components in the food products, such as proteins[42−44] and flavor compounds.[45] $MgCl_2$ and $CaCl_2$ have a bitter and salty taste,[30,46] which can be unwanted in a product. Encapsulation of mineral salts can be applied to improve their stability and reduce reactions with other components in the food products.[31−33,36,47,48] Dispersion of submicrometer salt particles in oil is also an encapsulation method and results in a slow release system which may reduce their bitter off-taste and reactions with other components.

There are various methods to produce submicrometer particles of salts, but many of these methods have shortcomings: most methods result in nonfood-grade particles, size control can be a problem, and redispering the particles may be difficult. In this paper a method is described for preparing food-grade submicrometer salt particles using ethanol-in-oil (E/O) mixtures. The method results in particles in the submicrometer size range that remain suspended in the oil phase, which allows instant use without the need of resuspending them.[29,49]

A common method to produce submicrometer particles from water-soluble salts uses a w/o microemulsion, carrying a water-soluble salt in the water phase. Subsequently, both phases (water and apolar solvent) are evaporated. By removing water from the micelles, salt/surfactant composites are formed, which can be resuspended in an apolar solvent.[50,51] Preparation of submicrometer particles of water-soluble salts through evaporation of the liquid phases from the w/o microemulsion has been described extensively in the literature.[50−57] Typically water is used as a polar solvent, heptane is used as an apolar solvent, and dioctyl sodium sulfosuccinate (AOT) is applied as surfactant. Heptane is also often used as apolar phase for redispersing the submicrometer particles. The toxicity of solvents such as heptane makes the resulting submicrometer particle method unpractical for applications in food. To produce food-grade submicrometer particles from water-soluble salts, food-grade solvents and surfactants should be used.

Water-soluble food-grade submicrometer particles can also be obtained with spray-drying techniques.[58] Although this method can result in food-grade submicrometer particles,

Received: May 25, 2012
Revised: July 31, 2012
Accepted: August 2, 2012
Published: August 2, 2012

subsequent dispersing in suitable food-grade oil remains a challenging task. In our method this dispersion step is no longer necessary.

Our method uses only food-grade materials and does not require evaporation of the continuous (apolar) phase. Medium-chain triglyceride (MCT) oil is used as a nonvolatile apolar continuous phase, and ethanol is used as dispersed phase instead of water. Ethanol is (partly) soluble in the MCT oil[59] and can be evaporated more easily than water, which also results in a faster method for obtaining submicrometer particles. Submicrometer particles remain suspended in the oil phase, which allows instant use without the need of resuspending them in a suitable (food-grade) oil phase.

MATERIALS AND METHODS

Safety: Due to the toxicity of hexane and since it is a volatile solvent, the washing step with hexane was performed in a fume hood. Since ethanol is a flammable solvent, its evaporation from the MCT oil phase was performed on a heating plate only and samples were not exposed to open flames.

Materials. Calcium chloride dihydrate (GR for analyses, Merck, ≥99%), ethanol absolute (Merck, ≥99.2%), Grindsted polyglycerol polyricinoleate (PGPR) 90 kosher (Danisco), *n*-hexane (p.a., Merck, ≥99%), magnesium chloride hexahydrate (GR, Merck, ≥99%), and a medium-chain triglyceride (MCT) oil (Miglyol 812 N, Sasol) were used as received.

Method for Production of Submicrometer Particles. Various molal solutions (0.1, 0.5, and 1.0 *m*) of the ethanol-soluble salts ($CaCl_2{\cdot}2H_2O$, $MgCl_2{\cdot}6H_2O$) were prepared in ethanol. After complete dissolution of the salts the solutions were added, while stirring with a magnetic stirrer, in volume ratios up to 30% to a continuous phase of MCT oil containing either 4% (w/w) PGPR or 6% (w/w) PGPR as surfactant. Samples were then sonicated using a Branson Sonifier 250 (output control level 6, duty cycle 60%) for 1 min to form an E/O mixture. Ethanol was evaporated from the samples by heating them overnight while stirring. After all ethanol was evaporated, samples were cooled to room temperature in a desiccator containing nitrogen gas and a desiccant. Samples were kept in closed containers and stored in the desiccator until further analyses.

Stability of Ethanol-in-Oil Mixtures. The stability of the created E/O mixtures was analyzed directly after sonication of the samples. Samples were visually examined, and their stability against creaming and coalescence was examined by multiple light scattering (MLS) using a Turbiscan ma2000 (Formulaction SA, L'Union, France).

Size Characterization of Initial Emulsion Droplets. The size and size distribution of the emulsion droplets in the E/O mixtures were analyzed directly after sonication of the samples. Samples were therefore analyzed by dynamic light scattering (DLS) with a ZetasizerNano ZS (Malvern Instruments Ltd., Worcestershire, U.K.)in a square glass cell (Malvern PCS1115).

Size and Size Distribution of Salt Particles. Dynamic light scattering (DLS) was used to examine the size and size distributions of the salt particles, formed after evaporation of the ethanol phase, with a Zetasizer Nano ZS (Malvern Instruments Ltd., Worcestershire, U.K.). Undiluted as well as diluted samples (2 and 3 times with MCT oil containing PGPR) were analyzed. All samples were analyzed in a square glass cell (Malvern PCS1115). Samples were measured at 20 °C, and a refractive index of 1.449 was used for MCT oil (product specifications). Refractive indices for the salts were set to 1.520 for $CaCl_2$[60] and 1.59 for $MgCl_2$.[60]

Morphology of Submicrometer Particles by SEM. MCT oil and surfactant were removed from the sample before characterizing the submicrometer particles with the SEM. Washing was performed by adding hexane to the samples and centrifuging them at 4000*g* for 10 min in a Thermo Scientific centrifuge (Heraeus Multifuge X3R). Supernatant was removed, and the pellet containing the submicrometer particles was redispersed in hexane. This washing step was repeated 3 times. After the washing step the washed submicrometer salt particles, dispersed in 5 mL of hexane, were sonicated for 10 min in a sonication bath. A drop of this dispersion was put on a Nuclepore Track-Etched Membrane (Whatman, 13 mm circular, 5 μm pores) and transferred into a sputter coater (Balzers SCD 020), where it was dried under vacuum. It was subsequently sputter coated with gold (3 min, 35 kA, 0.2 mBar argon). Samples were analyzed at room temperature in a scanning electron microscope (Jeol JAMP-9500F, Wageningen, The Netherlands). Images were digitally recorded.

Morphology of Submicrometer Particles by Cryo-SEM. MCT oil and surfactant were removed from the sample before characterizing the submicrometer particles with cryo-SEM. Washing was performed by adding hexane to the samples and centrifuging them at 50 000*g* for 20 min in a Beckman Coulter Avanti J-26 XP centrifuge. Supernatant was removed, and the pellet containing the submicrometer particles was redispersed in hexane. This washing step was repeated 3 times. Sample, dispersed in 5 mL of hexane, was then sonicated for 10 min in a sonication bath. Sample was put on clean (plasma glowed) coverslips and air dried at room temperature. Coverslips (8 mm circular, Menzel, Brauschweig, Germany) were glued on a sample holder by carbon glue (Leit-C, NeubauerChemicalien, Germany) and frozen at a liquid nitrogen (LN_2) cooled block. The sample holder was transferred to a nondedicated cryo-preparation system (MED 020/VCT 100, Leica, Vienna, Austria) onto a sample stage at −93 °C. In this cryo-preparation chamber the samples were freeze dried for 2 min at −93 °C at 1.3×10^{-6} mbar to remove water vapor contamination. Sample was sputter coated with a layer of 5 nm tungsten at the same temperature. Samples were cryo-shielded transferred into the field emission scanning microscope (Magellan 400, FEI, Eindhoven, The Netherlands) on the sample stage at −122 °C at 4×10^{-7} mbar. Analysis was performed at a working distance of 4 mm, with SE and BSE detection at 2−15 kV, 25 pA. All images were recorded digitally.

RESULTS AND DISCUSSION

Characterization of Ethanol-in-Oil Mixtures. Stability was evaluated by visual observations and MLS. The stability of mixtures of ethanol, containing $CaCl_2{\cdot}2H_2O$ (further named $CaCl_2$) or $MgCl_2{\cdot}6H_2O$ (further named $MgCl_2$), in MCT oil containing PGPR as surfactant was examined for 8 h. It was found that the volume percentage of ethanol added and the concentration of salt in the ethanol phase influenced the stability and appearance of the samples. An overview of visual observations and conclusions from the MLS measurements is given in Table 1. In Figures 1 and 2 some typical results from samples containing calcium and magnesium salts measured by MLS are presented.

Table 1 shows that depending on the salt concentration and volume percentage of ethanol added to the oil phase, either a transparent system was formed or an opaque one. These systems appeared transparent or opaque directly after mixing the ethanol phase with MCT oil, and in several of the systems stability issues occurred during the 8 h analyses. In general, it was found for both $CaCl_2$ and $MgCl_2$ that an increase in salt concentrations and/or increase in ethanol concentrations results in a decrease in the stability of the mixture and can cause the mixture to become opaque. From Table 1 it can be seen that samples containing $MgCl_2$ have a less wide stability window than samples containing $CaCl_2$. When pure ethanol was added in different volume concentrations to the MCT oil containing PGPR it resulted in transparent and stable mixtures. This shows that the stability of the E/O mixtures is strongly affected by the salt concentration.

From a chemical point of view it is known that ethanol can, due to its amphiphilic nature, dissolve to a certain extent in MCT oil.[59] However, the presence of water and impurities in the ethanol phase reduces its solubility in oil. As described above, it was found that addition of different volume concentrations of pure ethanol to MCT oil resulted in

Table 1. Effect of Salt Concentration, Ethanol Concentration, and PGPR Concentration on Sample Appearance and Stability[a]

MCT		ethanol (% v/v)	salt concentration (in EtOH) 0.1 *m*	0.5 *m*	1.0 *m*
MCT + 4% (w/w) PGPR	$CaCl_2 \cdot 2H_2O$	5	T	T	T
			S	S	S
		10	T	O	O
			S	U (C)	U (C + P)
		20	T	O	O
			S	U (C + P)	U (C + P)
		30	T	O	O
			S	U (C + P)	U (C + P)
MCT + 6% (w/w) PGPR	$CaCl_2 \cdot 2H_2O$	5	T	T	T
			S	S	S
		10	T	O	O
			S	U (C + P)	U (C + P)
		20	T	O	O
			S	U (C + P)	U (C + P)
		30	T	O	O
			S	U (C + P)	U (C + P)
MCT + 4% (w/w) PGPR	$MgCl_2 \cdot 6H_2O$	5	T	O	O
			S	U (C)	U (C)
		10	T/O	O	O
			S	U (C)	U (P)
		20	O	O	O
			U (C + P)	U (C + P)	U (C + P)
		30	T	O	O
			S	U (C + P)	U (C + P)
MCT + 6% (w/w) PGPR	$MgCl_2 \cdot 6H_2O$	5	T	O	O
			S	U (C)	U (C)
		10	T/O	O	O
			S	U (P)	S
		20	O	O	O
			U (C + P)	U (C + P)	U (C + P)
		30	T	O	O
			S	U (C + P)	U (C + P)

[a]Samples are examined for 8 h by visual observation and MLS measurement. Samples are created with 0.1, 0.5, or 1.0 m $CaCl_2 \cdot 2H_2O$ and $MgCl_2 \cdot 6H_2O$ in ethanol and mixed at 5%, 10%, 20%, or 30% (v/v) in MCT oil containing PGPR. Explanation of symbols: T = transparent, O = opaque, S = stable, U = unstable (with C = coalescence and P = phase separation).

transparent and stable mixtures (visual examination for 24 h). When low concentrations of $CaCl_2$ or $MgCl_2$ were present in the ethanol phase, transparent and stable mixtures were also obtained with MCT oil (Table 1). The PGPR seemed not required in these transparent mixtures since they remained visually stable during 24 h. At sufficiently high salt concentrations phase separation appeared to occur, in which the system most likely separated into droplets of an ethanol-rich phase in an oil-rich continuous phase, and PGPR (at least partially) stabilizes the droplets. In the absence of PGPR, the unstable system phase separated almost instantly. Phase separation was influenced by temperature: a higher salt concentration was required for inducing phase separation at elevated temperature. The phase diagram of ethanol and MCT oil with the presence of $CaCl_2$ or $MgCl_2$ was not fully characterized, since this is outside the scope of the present study. Therefore, it is uncertain which amount of ethanol is mixed with the MCT oil and which amount is present as a separate phase.

In Figure 1a data from the MLS measurements of samples created with 5% (v/v) 1.0 *m* $CaCl_2 \cdot 2H_2O$ in ethanol added to MCT oil is given. Each line represents the same sample measured at different times. The horizontal profile of the lines in Figure 1a is similar to each other, from which can be concluded that this sample is stable for 8 h. In Figure 1b the data is given for a sample where $MgCl_2 \cdot 6H_2O$ is used instead. The lines in Figure 1b have a similar horizontal profile but with different intensity. The back-scattering percentage changes evenly over the entire sample height. It is interpreted that this change in back scattering is caused by a change in droplet size and indicates that the sample is not stable over time. After 24 h it was also noticed that phase separation has occurred in the sample with $MgCl_2$. Looking at a certain sample height gives a better impression of the trend of the change in droplet size. In Figure 1c the data from Figure 1a and 1b are combined into one figure and results are shown only for the back scattering at a sample height of 30 mm. In order to observe the effect of PGPR concentration, samples containing 6% (w/w) PGPR in MCT oil are presented here as well. For samples with $CaCl_2$, shown in Figure 1c, no change in droplet size occurs for 8 h. Samples with $MgCl_2$ are unstable, as concluded from Figure 1b, and the change in droplet size results in a decrease of the back-scattering signal. The change in droplet size in the sample with $MgCl_2$ is most likely caused by coalescence. However, disproportionation (Ostwald ripening) may also play a large role here due to the solubility of ethanol in MCT oil. From Figure 1c no clear effect can be observed when increasing the PGPR concentration from 4% (w/w) to 6% (w/w) PGPR.

In Figure 2a the data from the MLS measurements of samples created with 20% (v/v) 1.0 *m* $MgCl_2 \cdot 6H_2O$ in ethanol added to MCT oil is given. From Figure 2a it can be seen that the sample is very unstable over time. The peak at about 10 mm sample height indicates formation of a transparent oil-rich layer (bottom of sample), and at about 60 mm sample height (top of sample) a transparent ethanol-rich layer is formed, clearly indicating the system is phase separating. Figure 2a also shows a partly horizontal profile (between 11 and 40 mm sample height) where only the back-scattering percentage changes evenly over time. This is an indication for a change in droplet size, and the corresponding trend, represented by an ascending line, at a sample height of 30 mm is shown in Figure 2b. In order to see the effect of PGPR a similar sample produced in MCT oil containing 6% (w/w) PGPR is shown here as well. Both samples give a comparable ascending line, which shows that addition of extra PGPR to the sample did not affect the change in droplet size. Also, for other samples no significant effect on the stabilization of the mixtures by an increased PGPR concentration could be observed.

Size Characterization of Initial Emulsion Droplets. E/O mixtures with $CaCl_2$ or $MgCl_2$ dissolved in the ethanol phase

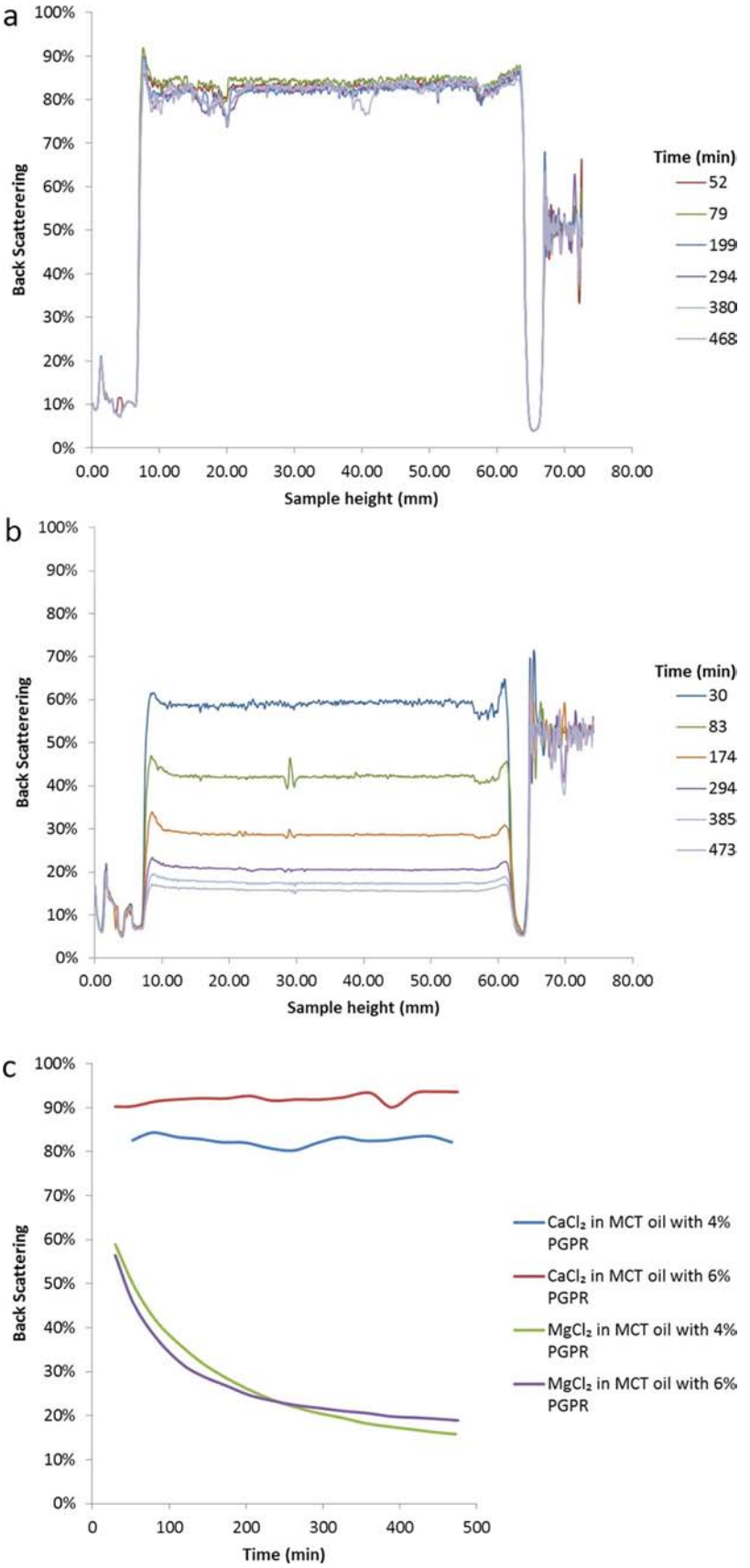

Figure 1. Typical MLS results from a stable sample and sample that changes over time. (a) Sample created with 1.0 *m* $CaCl_2 \cdot 2H_2O$ in ethanol and mixed at 5% (v/v) in MCT oil containing 4% (w/w) PGPR. Sample is monitored for 8 h. (b) Sample created with 1.0 *m* $MgCl_2 \cdot 6H_2O$ in ethanol and mixed at 5% (v/v) in MCT oil containing 4% (w/w) PGPR. (c) Back scattering at a sample height of 30 mm for samples from a and b. Variations with 6% (w/w) PGPR are presented here as well.

dx.doi.org/10.1021/jf3023029 | *J. Agric. Food Chem.* 2012, 60, 8501−8509

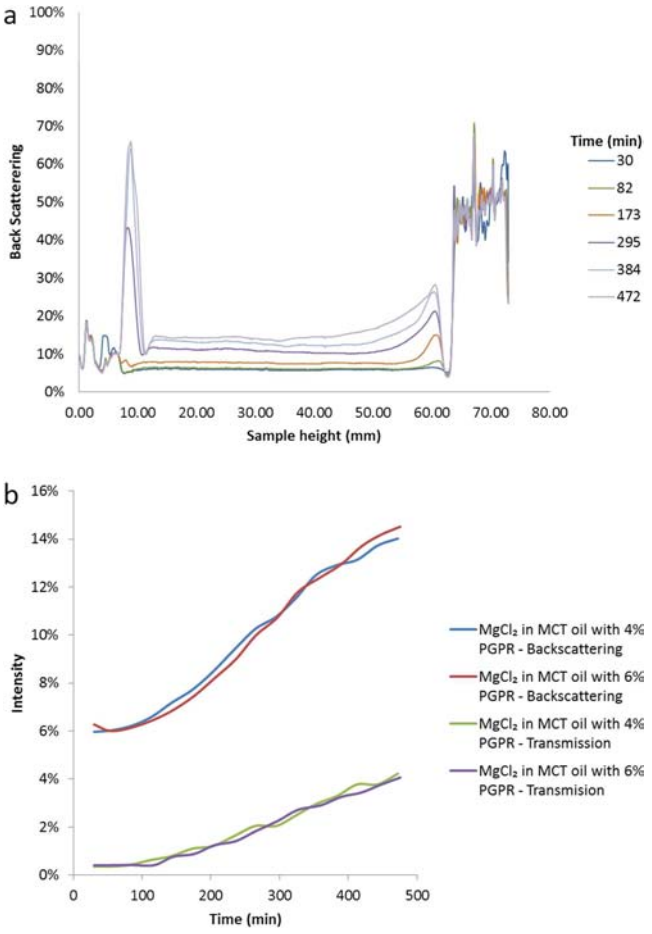

Figure 2. Typical MLS results from an unstable sample containing $MgCl_2 \cdot 6H_2O$. (a) Sample created with 1.0 *m* $MgCl_2 \cdot 6H_2O$ in ethanol and mixed at 20% (v/v) in MCT oil containing 4% (w/w) PGPR. Sample is monitored for 8 h. (b) Backscattering and transmission trend at a sample height of 30 mm for the sample from a. Variation with 6% (w/w) PGPR is presented here as well.

were analyzed by DLS. Samples that appeared as transparent showed droplets with a diameter in the range from 20 to 160 nm. Opaque mixtures contained droplets with a diameter in the range of 600−1400 nm. In the latter one the large emulsion droplets masked the smaller droplets. The instability of the opaque mixtures made DLS analyses less reliable for size characterization of the emulsion droplets in these samples.

Characterization of Salt Particles after Evaporation of Ethanol. *Size and Size Distribution of Salt Particles.* Samples containing salt particles were further analyzed with DLS to investigate the presence of submicrometer particles. In Table 2 an overview is given from the DLS measurements. In all samples submicrometer particles could be observed, but samples that appeared as opaque contain also many larger particles. This made the formulations used in these opaque mixtures less useful for production of salt submicrometer particles.

DLS measurements showed the presence of submicrometer salt particles in all samples prepared with $CaCl_2$ and $MgCl_2$. Samples appeared as transparent or opaque, as described in Table 2. Transparent samples contained mainly salt particles with an average below 300 nm, and only a negligible amount of larger salt particles was present. The opaque samples contained salt particles smaller than 400 nm but also a considerable amount of large particles, causing an opaque appearance. These large salt particles could be observed with a light microscope. The opaque samples were difficult to measure with DLS because of the wide size distribution of the salt particles. The larger salt particles masked the smaller salt particles. Therefore, not all particle sizes are listed in Table 2. In some of the samples, for instance, 1.0 *m* $CaCl_2 \cdot 2H_2O$ and 5% (v/v) ethanol, salt crystals of 1−30 μm were found, but DLS measurements showed a peak average of 183 nm based on the size distribution by volume.

It is remarkable that with 0.1 *m* $CaCl_2 \cdot 2H_2O$ and 20% (v/v) ethanol mainly particles with an average size of 6 nm were found. A minor amount of large particles was found by DLS as well, which could also be observed by light microscopy. However, no clear peak around 200 nm could be observed with DLS. It is expected that the substantial amount of very small particles could be the result of Ostwald ripening in the sample. Since ethanol is soluble in MCT oil, Ostwald ripening can easily take place and due to a higher content of ethanol in the sample it is likely to be more unstable compared to samples with a lower ethanol concentration. Ostwald ripening is the effect where larger droplets grow at the expense of the small ones, and the small droplets become even smaller. Evaporation of these smaller droplets could result then in smaller particles as well. This could be an explanation for a shift of the peak around 200 nm to the left and right, as observed in Figure 3. Particles around 10 nm were also found in other samples containing lower concentrations of ethanol, but these did not show up clearly with DLS.

From the E/O mixtures described in Table 1 and the salt particles described in Table 2 it can be concluded that only transparent E/O mixtures were successful in producing salt submicrometer particles with a minimal number of larger particles. Samples with 0.1 *m* salt and 30% (v/v) ethanol resulted also in a transparent mixture; however, after evaporation of the ethanol phase the sample became opaque and large particles and crystals could be observed. The same holds for the sample with 1.0 *m* $CaCl_2 \cdot 2H_2O$ and 5% (v/v) ethanol, which appeared transparent as a mixture but became opaque after evaporation of the ethanol phase. During production of the particles, ethanol is removed from the system and the relative concentration of salt in ethanol is therefore increasing. If this relative salt concentration is too high the mixture becomes unstable. Full characterization of the phase diagram of ethanol and MCT oil with the presence of $CaCl_2$ or $MgCl_2$ can give better insight on how the systems shift through the phase diagram during evaporation of ethanol, but this is outside the scope of the present study. Small emulsion droplets or even solutions of ethanol in MCT oil are useful for formation of submicrometer particles. However, having instable mixtures where coalescence and/or phase separation occurs reduces the chance to form submicrometer particles and more large particles and crystals will be obtained.

In general, it was found that increasing the volume percentage of ethanol and/or increasing the concentration of salt shows that the number of large particles increases and also the size of the large particles increases. An increase in volume percentage of ethanol and/or salt concentration results also in a more polydisperse size distribution of the salt particles. Samples prepared with $MgCl_2$ have a less wide concentration window for formation of submicrometer particles with a minimal amount of larger particles, compared to samples prepared with $CaCl_2$.

Table 2. Overview of Samples Containing Salt Particles Measured by DLS (using a Nanosizer)[a]

			salt concentration (in EtOH)		
MCT		ethanol (% v/v)	0.1 *m*	0.5 *m*	1.0 *m*
MCT + 4% (w/w) PGPR	$CaCl_2 \cdot 2H_2O$	5	transparent 203.7 nm (100%)	transparent 173.4 nm (80.2%) 1281.3 nm (19.9%)	opaque 183.4 nm (100%)
		10	transparent 231.8 nm (100%)	opaque	opaque
		20	transparent 6.1 nm (97.4%) 895.4 nm (0.9%) 3549.5 nm (1.7%)	opaque	opaque
		30	opaque	opaque	opaque
MCT + 4% (w/w) PGPR	$MgCl_2 \cdot 6H_2O$	5	transparent 215.9 nm (100%)	opaque 1175.3 nm (53.3%) 3083.4 nm (46.7%)	opaque 90.2 nm (5.4%) 1156.7 nm (94.6%)
		10	semi-transparent 315.2 nm (100%)	opaque	opaque
		20	opaque 93.3 nm (51.3%) 493.5 nm (48%) 3037.8 nm (0.3%)	opaque	opaque
		30	opaque	opaque	opaque
MCT + 6% (w/w) PGPR	$MgCl_2 \cdot 6H_2O$	5	transparent 337.3 nm (100%)	opaque 250.1 nm (100%)	opaque 438.3 nm (92.4%) 3595.5 nm (7.6%)
		10	semi-transparent 341.2 nm (98.8%) 1397.5 nm (1.2%)	opaque	opaque
		20	semi-transparent 770.1 nm (88.6%) 4109.8 nm (11.5%)	opaque	opaque
		30	opaque	opaque	opaque

[a]Sample appearance, transparent or opaque, is given. Size represents the peak average based on size distribution by volume; the percentages represent the peak area. Samples are created with 0.1, 0.5, or or 1.0 *m*$CaCl_2 \cdot 2H_2O$ and $MgCl_2 \cdot 6H_2O$ in ethanol and mixed at 5%, 10%, 20%, or 30% (v/v) in MCT oil containing PGPR. Ethanol phase has been evaporated at 60 °C, resulting in formation of micro- and submicrometer salt particles.

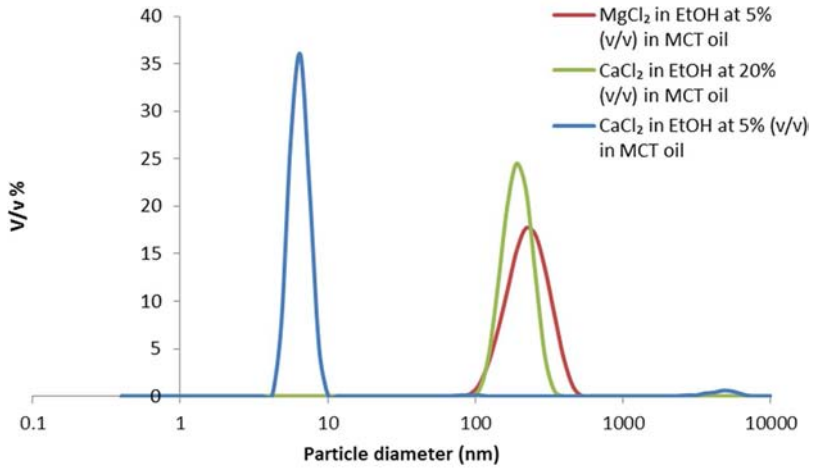

Figure 3. Size distribution by volume percentage, measured by DLS, of samples with 0.1 *m* salt and mixed at 5% and 20% (v/v) ethanol in MCT oil containing 4% (w/w) PGPR. Ehanol was evaporated at 60 °C.

It was found that some of the transparent E/O mixtures were stable without the presence of PGPR. It was therefore investigated if some of these transparent mixtures were also suitable to form salt submicrometer particles in the absence of PGPR. Samples containing 0.1 *m* $CaCl_2 \cdot 2H_2O$ with 5−20% (v/v) ethanol in MCT oil and a sample containing 0.5 *m* $CaCl_2 \cdot 2H_2O$ with 5% (v/v) ethanol in MCT oil were prepared. None of these samples contained PGPR as surfactant, and transparent mixtures were obtained. Ethanol was evaporated from the MCT oil phase at 60 °C during 14 h, and samples

were visually characterized and analyzed by a microscope. It was found that large crystals and salt particles were obtained, and particles also clustered together in samples prepared without PGPR. On the other hand, similar samples but with PGPR did result in submicrometer salt particles. It can be concluded from this that a surfactant such as PGPR is required in formation and stabilization of submicrometer salt particles. Surfactant molecules, which are predominantly adsorbed on the surface of the submicrometer particle, are expected to have an important role in controlling the submicrometer particle size and stabilizing their suspension.[50,51] It was also observed that an increase in PGPR concentration reduced the amount of large particles that were formed. For instance, a sample with 0.1 *m* $MgCl_2 \cdot 6H_2O$ and 20% (v/v) ethanol is more transparent when 6% (w/w) PGPR is used than when 4% (w/w) PGPR is used. Light microscopy of the sample with 6% (w/w) PGPR revealed fewer large particles compared to the sample with 4% (w/w) PGPR.

Figure 3 shows the size distribution by volume, measured by DLS, of salt particles produced from 0.1 *m* salt and mixed at 5% and 20% (v/v) ethanol in MCT oil containing 4% (w/w) PGPR. In Figure 3 only one peak around 200 nm can be observed for samples prepared with 5% (v/v) ethanol. Sample prepared with 20% (v/v) ethanol shows two peaks, one major peak around 6 nm and another minor peak around 4800 nm. As explained above, it is expected that this shift is due to Ostwald ripening.

Morphology of Submicrometer Particles. The morphology of the formed salt submicrometer particles was studied with SEM and Cryo-SEM. In Figure 4 micrographs from the SEM and Cryo-SEM of salt submicrometer particles are shown.

In Figure 4 it can clearly be seen that submicrometer salt particles of various sizes below 400 nm were obtained. Figure 4a and 4b shows $CaCl_2$ submicrometer particles of about 100 nm observed with the Auger/SEM. In Figure 4c and 4d a similar sample is represented but observed with the Cryo-SEM and a few large (270 nm) but also a considerable number of much smaller (20−60 nm) salt particles were found. The washing step applied to the samples shown in Figure 4a and 4b and Figure 4c and 4d differed and is an explanation for the observed differences. The sample from Figure 4c and 4d was centrifuged at much higher speed (50 000*g* for 30 min versus 4000*g* for 10 min for the sample in Figure 4a and 4b). Therefore, more small $CaCl_2$ particles ended up in the pellet due to the higher centrifugation forces. Comparison of the results from $CaCl_2$ shows that the upper range (<342 nm) is quite comparable to what was found with SEM and Cryo-SEM (Figure 3). However, the lower range (<90 nm) is not really visible in Figure 3 for $CaCl_2$, whereas with Cryo-SEM several particles below 90 nm could clearly be seen. This could confirm that the larger particles mask the smaller ones, and therefore, the particles below 90 nm are not observed with DLS measurements. It must be noted that samples from Figure 3 were created with 4% (w/w) PGPR and the samples from Figure 4 were created with 6% (w/w) PGPR. Figure 4e and 4f shows submicrometer particles of $MgCl_2$ which are in a size range of 300−400 nm. According to the DLS results shown in Figure 3, much smaller particles must be present as well. It is expected that these smaller $MgCl_2$ particles were removed during the washing step, as also concluded for the sample in Figure 4a and 4b. All submicrometer salt particles observed with SEM and Cryo-SEM seemed to be cubical, and this suggests that the particles have a cubic crystal structure.

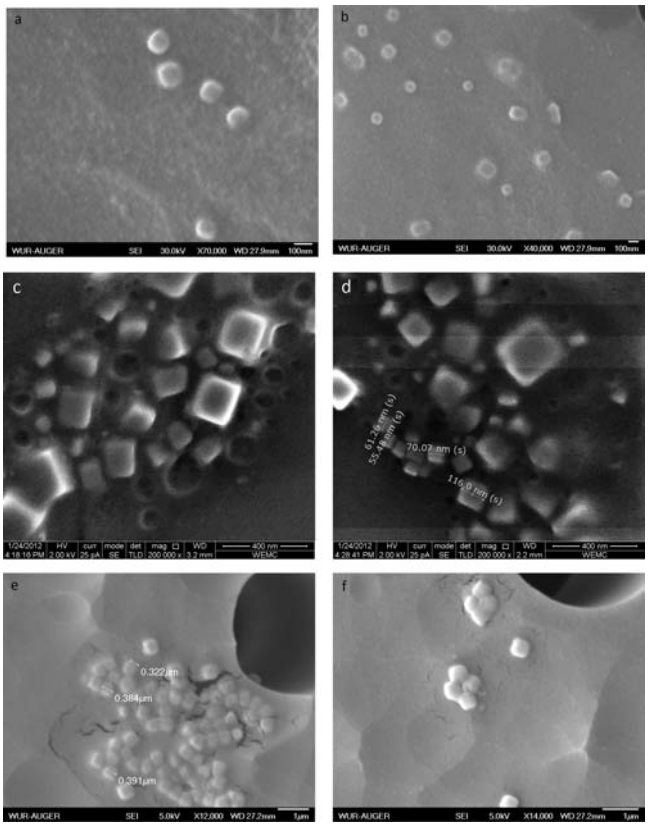

Figure 4. Submicrometer salt particles analyzed with SEM and Cryo-SEM. (a and b) $CaCl_2$ submicrometer salt particles observed with Auger/SEM [Sample created with 0.1 *m* $CaCl_2 \cdot 2H_2O$ in ethanol and mixed at 5% (v/v) in MCT oil containing 6% (w/w) PGPR. Ethanol was evaporated at 60 °C. Sample has been washed with hexane to remove oil and surfactant]. (c and d) $CaCl_2$ submicrometer salt particles observed with Cryo-SEM [Sample created with 0.1 *m* $CaCl_2 \cdot 2H_2O$ in ethanol and mixed at 5% (v/v) in MCT oil containing 6% (w/w) PGPR. Ethanol was evaporated at 60 °C. Sample has been washed with hexane to remove oil and surfactant]. (e and f) $MgCl_2$ submicrometer salt particles observed with Auger/SEM [Sample created with 0.1 *m* $MgCl_2 \cdot 6H_2O$ in ethanol and mixed at 5% (v/v) in MCT oil containing 6% (w/w) PGPR. Ethanol was evaporated at 60 °C. Sample has been washed with hexane to remove oil and surfactant].

It can be concluded that our simple method for preparing food-grade salts particles in the submicrometer range is successful. Salt particles were prepared from ethanol-soluble salts using ethanol-in-oil (E/O) mixtures. It was found that increasing the salt concentration ($CaCl_2$ and $MgCl_2$) and ethanol concentration reduced the stability of the obtained mixtures. Also, the type of salt ($CaCl_2$ or $MgCl_2$) influenced the stability of the mixture. MLS measurements showed that transparent mixtures remained stable for at least 8 h and opaque mixtures were found to be unstable during these 8 h. PGPR was required in these unstable systems to partly stabilize the droplets, whereas the absence of PGPR resulted in an almost instant phase separation in these systems. No significant effect on the stability of the mixtures could be observed when increasing the PGPR concentration from 4% (w/w) to 6% (w/w) PGPR.

It can also be concluded that salt particles with dimensions in the submicrometer range (6−400 nm) were obtained in all samples after evaporation of the ethanol phase, but only the

samples that appeared as "transparent E/O mixture" were successful in forming salt submicrometer particles with a minimum of larger salt particles present. The concentration of salt and volume fraction of ethanol was found to have a significant influence on the size distribution of salt particles. It was also found that PGPR was required not only to obtain more stable mixtures of ethanol and MCT oil but also in formation and stabilization of submicrometer salt particles.

The developed method is based on the use of food-grade materials, and the obtained submicrometer particles are therefore regarded as food safe. This increases the range of applications and makes application of these submicrometer particles in food products possible, thereby supporting development of new advanced food products.

AUTHOR INFORMATION

Corresponding Author

*Tel.: 0031-317-485023. Fax: 0031-317-483669. E-mail leonard.sagis@wur.nl.

Notes

The authors declare no competing financial interest.

ACKNOWLEDGMENTS

The authors express their gratitude to Dr. Adriaan van Aelst for the assistance during Cryo-SEM measurements and MicroNed is gratefully acknowledged for their financial support.

ABBREVIATIONS USED

Cryo-SEM, cryo scanning electron microscope; DLS, dynamic light scattering; E/O mixture, ethanol in oil mixture; m, molal; MCT oil, medium chain triglyceride oil; MLS, multiple light scattering; PGPR, polyglycerol polyricinoleate; SEM, scanning electron microscope; % (v/v), volume percentage; % (w/w), weight percentage

REFERENCES

(1) Corot, C.; Robert, P.; Idée, J. M.; Port, M. Recent advances in iron oxide nanocrystal technology for medical imaging. *Adv. Drug Delivery Rev.* **2006**, *58*, 1471−1504.

(2) Boisselier, E.; Astruc, D. Gold nanoparticles in nanomedicine: Preparations, imaging, diagnostics, therapies and toxicity. *Chem. Soc. Rev.* **2009**, *38*, 1759−1782.

(3) Mornet, S.; Vasseur, S.; Grasset, F.; Duguet, E. Magnetic nanoparticle design for medical diagnosis and therapy. *J. Mater. Chem.* **2004**, *14*, 2161−2175.

(4) Pyrzynska, K. Carbon nanostructures for separation, preconcentration and speciation of metal ions. *TrAC, Trends Anal. Chem.* **2010**, *29*, 718−727.

(5) Park, S. J.; Taton, T. A.; Mirkin, C. A. Array-based electrical detection of DNA with nanoparticle probes. *Science* **2002**, *295*, 1503−1506.

(6) Kokura, S.; Handa, O.; Takagi, T.; Ishikawa, T.; Naito, Y.; Yoshikawa, T. Silver nanoparticles as a safe preservative for use in cosmetics. *Nanomedicine* **2010**, *6*, 570−574.

(7) Sambhy, V.; MacBride, M. M.; Peterson, B. R.; Sen, A. Silver bromide nanoparticle/polymer composites: Dual action tunable antimicrobial materials. *J. Am. Chem. Soc.* **2006**, *128*, 9798−9808.

(8) Sanguansri, P.; Augustin, M. A. Nanoscale materials development - a food industry perspective. *Trends Food Sci. Technol.* **2006**, *17*, 547−556.

(9) Weiss, J.; Takhistov, P.; McClements, D. J. Functional materials in food nanotechnology. *J. Food Sci.* **2006**, *71*, R107−R116.

(10) Chaudhry, Q.; Scotter, M.; Blackburn, J.; Ross, B.; Boxall, A.; Castle, L.; Aitken, R.; Watkins, R. Applications and implications of nanotechnologies for the food sector. *Food Addit. Contam., Part A* **2008**, *25*, 241−258.

(11) Isobe, H.; Utsumi, S.; Yamamoto, K.; Kanoh, H.; Kaneko, K. Micropore to Macropore Structure-Designed Silicas with Regulated Condensation of Silicic Acid Nanoparticles. *Langmuir* **2005**, *21*, 8042−8047.

(12) Gong, Q.; Qian, X.; Zhou, P.; Yu, X.; Du, W.; Xu, S. In situ sacrificial template approach to the synthesis of octahedral CdS microcages. *J. Phys. Chem. C* **2007**, *111*, 1935−1940.

(13) Luechinger, N. A.; Walt, S. G.; Stark, W. J. Printable nanoporous silver membranes. *Chem. Mater.* **2010**, *22*, 4980−4986.

(14) Calogero, G.; Calandra, P.; Sinopoli, A.; Gucciardi, P. G., Metal nanoparticles and carbon-based nanostructures as advanced materials for cathode application in dye-sensitized solar cells. *Int. J. Photoenergy* **2010**,*2010*.

(15) Shipway, A. N.; Katz, E.; Willner, I. Nanoparticle arrays on surfaces for electronic, optical, and sensor applications. *ChemPhysChem* **2000**, *1*, 18−52.

(16) Trindade, T.; O'Brien, P.; Pickett, N. L. Nanocrystalline semiconductors: Synthesis, properties, and perspectives. *Chem. Mater.* **2001**, *13*, 3843−3858.

(17) Kamat, P. V. Photophysical, photochemical and photocatalytic aspects of metal nanoparticles. *J. Phys. Chem. B* **2002**, *106*, 7729−7744.

(18) Murphy, C. J.; Sau, T. K.; Gole, A. M.; Orendorff, C. J.; Gao, J.; Gou, L.; Hunyadi, S. E.; Li, T. Anisotropic metal nanoparticles: Synthesis, assembly, and optical applications. *J. Phys. Chem. B* **2005**, *109*, 13857−13870.

(19) Biju, V.; Itoh, T.; Anas, A.; Sujith, A.; Ishikawa, M. Semiconductor quantum dots and metal nanoparticles: Syntheses, optical properties, and biological applications. *Anal. Bioanal. Chem.* **2008**, *391*, 2469−2495.

(20) Koh, W. G.; Revzin, A.; Pishko, M. V. Poly(ethylene glycol) hydrogel microstructures encapsulating living cells. *Langmuir* **2002**, *18*, 2459−2462.

(21) Anna, S. L.; Bontoux, N.; Stone, H. A. Formation of dispersions using "flow focusing" in microchannels. *Appl. Phys. Lett.* **2003**, *82*, 364−366.

(22) Charcosset, C.; Fessi, H. Membrane emulsification and microchannel emulsification processes. *Rev. Chem. Eng.* **2005**, *21*, 1−32.

(23) Sugiura, S.; Oda, T.; Izumida, Y.; Aoyagi, Y.; Satake, M.; Ochiai, A.; Ohkohchi, N.; Nakajima, M. Size control of calcium alginate beads containing living cells using micro-nozzle array. *Biomaterials* **2005**, *26*, 3327−3331.

(24) Choi, C. H.; Jung, J. H.; Rhee, Y. W.; Kim, D. P.; Shim, S. E.; Lee, C. S. Generation of monodisperse alginate microbeads and in situ encapsulation of cell in microfluidic device. *Biomed. Microdevices* **2007**, *9*, 855−862.

(25) Lin, Y. H.; Chen, C. T.; Huang, L. L. H.; Lee, G. B. Multiple-channel emulsion chips utilizing pneumatic choppers for biotechnology applications. *Biomed. Microdevices* **2007**, *9*, 833−843.

(26) Sugiura, S.; Oda, T.; Aoyagi, Y.; Matsuo, R.; Enomoto, T.; Matsumoto, K.; Nakamura, T.; Satake, M.; Ochiai, A.; Ohkohchi, N.; Nakajima, M. Microfabricated airflow nozzle for microencapsulation of living cells into 150 micrometer microcapsules. *Biomed. Microdevices* **2007**, *9*, 91−99.

(27) Zhang, H.; Tumarkin, E.; Sullan, R. M. A.; Walker, G. C.; Kumacheva, E. Exploring microfluidic routes to microgels of biological polymers. *Macromol. Rapid Commun.* **2007**, *28*, 527−538.

(28) Amici, E.; Tetradis-Meris, G.; de Torres, C. P.; Jousse, F. Alginate gelation in microfluidic channels. *Food Hydrocolloids* **2008**, *22*, 97−104.

(29) Liu, H.; Wang, C.; Gao, Q.; Liu, X.; Tong, Z. Fabrication of novel core-shell hybrid alginate hydrogel beads. *Int. J. Pharm.* **2008**, *351*, 104−112.

(30) Lawless, H. T.; Rapacki, F.; Horne, J.; Hayes, A. The taste of calcium and magnesium salts and anionic modifications. *Food Qual. Pref.* **2003**, *14*, 319−325.

(31) Zimmermann, M. B.; Wegmueller, R.; Zeder, C.; Chaouki, N.; Biebinger, R.; Hurrell, R. F.; Windhab, E. Triple fortification of salt with microcapsules of iodine, iron, and vitamin A. *Am. J. Clin. Nutr.* **2004**, *80*, 1283−1290.
(32) Romita, D.; Cheng, Y. L.; Diosady, L. L., Microencapsulation of ferrous fumarate for the production of salt double fortified with iron and iodine. *Int. J. Food Eng.* **2011**,7.
(33) Wegmüller, R.; Zimmermann, M. B.; Bühr, V. G.; Windhab, E. J.; Hurrell, R. F. Development, stability, and sensory testing of microcapsules containing iron, iodine, and vitamin A for use in food fortification. *J. Food Sci.* **2006**, *71*, S181−S187.
(34) Wang, J.; Chen, X.; Yang, X.; Xu, S.; Zhang, X.; Gou, Z. A facile pollutant-free approach toward a series of nutritionally effective calcium phosphate nanomaterials for food and drink additives. *J. Nanopart. Res.* **2011**, *13*, 1039−1048.
(35) Wegmüller, R.; Camara, F.; Zimmermann, M. B.; Adou, P.; Hurrell, R. F. Salt dual-fortified with iodine and micronized ground ferric pyrophosphate affects iron status but not hemoglobin in children in Côte d'Ivoire. *J. Nutr.* **2006**, *136*, 1814−1820.
(36) Sagalowicz, L.; Leser, M. E. Delivery systems for liquid food products. *Curr. Opin. Colloid Interface Sci.* **2010**, *15*, 61−72.
(37) Martin, B. R.; Weaver, C. M.; Heaney, R. P.; Packard, P. T.; Smith, D. L. Calcium absorption from three salts and CaSO 4-fortified bread in premenopausal women. *J. Agric. Food. Chem.* **2002**, *50*, 3874−3876.
(38) Perales, S.; Barberá, R.; Lagarda, M. J.; Farré, R. Fortification of milk with calcium: Effect on calcium bioavailability and interactions with iron and zinc. *J. Agric. Food. Chem.* **2006**, *54*, 4901−4906.
(39) Yew, J. Y.; Phillips, R. D.; Resurreccion, A. V. A.; Hung, Y. C. Physicochemical and sensory characteristic changes in fortified peanut spreads after 3 months of storage at different temperatures. *J. Agric. Food. Chem.* **2002**, *50*, 2377−2384.
(40) Schokker, E. P.; Dalgleish, D. G. Orthokinetic flocculation of caseinate-stabilized emulsions: Influence of calcium concentration, shear rate, and protein content. *J. Agric. Food. Chem.* **2000**, *48*, 198−203.
(41) Zeeb, B.; Fischer, L.; Weiss, J. Cross-linking of interfacial layers affects the salt and temperature stability of multilayered emulsions consisting of fish gelatin and sugar beet pectin. *J. Agric. Food. Chem.* **2011**, *59*, 10546−10555.
(42) Riou, E.; Havea, P.; McCarthy, O.; Watkinson, P.; Singh, H. Behavior of protein in the presence of calcium during heating of whey protein concentrate solutions. *J. Agric. Food. Chem.* **2011**, *59*, 13156−13164.
(43) Veerman, C.; Baptist, H.; Sagis, L. M. C.; Van der Linden, E. A new multistep CA 2+-induced cold gelation process for *β*-lactoglobulin. *J. Agric. Food. Chem.* **2003**, *51*, 3880−3885.
(44) Barbut, S.; Foegeding, E. A. Ca-induced gelation of pre-heated whey protein isolate2+. *J. Food Sci.* **1993**, *58*, 867−871.
(45) Bezman, Y.; Mayer, F.; Takeoka, G. R.; Buttery, R. G.; Ben-oliel, G.; Rabinowitch, H. D.; Naim, M. Differential effects of tomato (Lycopersicon esculentum Mill) matrix on the volatility of important aroma compounds. *J. Agric. Food. Chem.* **2003**, *51*, 722−726.
(46) Toelstede, S.; Hofmann, T. Quantitative studies and taste re-engineering experiments toward the decoding of the nonvolatile sensometabolome of Gouda cheese. *J. Agric. Food. Chem.* **2008**, *56*, 5299−5307.
(47) Ding, B.; Xia, S.; Hayat, K.; Zhang, X. Preparation and pH Stability of Ferrous Glycinate Liposomes. *J. Agric. Food. Chem.* **2009**, *57*, 2938−2944.
(48) Li, Y. O.; Diosady, L. L.; Wesley, A. S. Iodine stability in iodized salt dual fortified with microencapsulated ferrous fumarate made by an extrusion-based encapsulation process. *J. Food Eng.* **2010**, *99*, 232−238.
(49) Wang, C.; Liu, H.; Gao, Q.; Liu, X.; Tong, Z. Facile fabrication of hybrid colloidosomes with alginate gel cores and shells of porous CaCO3 microparticles. *ChemPhysChem* **2007**, *8*, 1157−1160.
(50) Marcianò, V.; Minore, A.; Turco Liveri, V. A simple method to prepare solid nanoparticles of water-soluble salts using water-in-oil microemulsions. *Colloid Polym. Sci.* **2000**, *278*, 250−252.
(51) Calandra, P.; Longo, A.; Turco Liveri, V. Preparation and characterisation of Na2S and ZnSO4 nanoparticles in water/sodium bis(2-ethylhexyl)sulphosuccinate/n-heptane microemulsions. *Colloid Polym. Sci.* **2001**, *279*, 1112−1117.
(52) Zhu, D. M.; Wu, X.; Schelly, Z. A. Reverse micelles and water in oil microemulsions of triton X-100 in mixed solvents of benzene and n-hexane. Dynamic light scattering and turbidity studies. *Langmuir* **1992**, *8*, 1538−1540.
(53) Giordano, C.; Longo, A.; Turco Liveri, V.; Venezia, A. M. Physicochemical investigation of the solubilization of cobalt nitrate in sodium bis(2-ethylhexyl)sulfosuccinate reversed micelles. *Colloid Polym. Sci.* **2003**, *281*, 229−238.
(54) Calandra, P.; Marco, G. D.; Ruggirello, A.; Liveri, V. T. Physico-chemical investigation of nanostructures in liquid phases: Nickel chloride ionic clusters confined in sodium bis(2-ethylhexyl) sulfosuccinate reverse micelles. *J. Colloid Interface Sci.* **2009**, *336*, 176−182.
(55) Fedorov, V. Y. Dispersity and growth kinetics of K2SO4 crystals in drops of an evaporating solution. *Tech. Phys.* **2009**, *54*, 656−660.
(56) Fedorov, V. Y. Calculation of the growth kinetics and dispersity of K2SO4 crystals in drops of an evaporating solution. *Tech. Phys.* **2010**, *55*, 972−980.
(57) Bulavchenko, A. I.; Arymbaeva, A. T.; Demidova, M. G.; Maksimovskii, E. A. Isothermal mass crystallization of ammonium and potassium nitrates from tergitol NP-4-based water-in-oil microemulsions. *Colloid J.* **2011**, *73*, 748−752.
(58) Tzu Ming Chen, H. M. C. Generation and Evaluation of Monodisperse Sodium Chloride and Oleic Acid Nanoparticles. *Aerosol Air Qual. Res.* **2006**, *6*, 17.
(59) Teng, S. X.; Wang, S. G.; Liu, X. W.; Gong, W. X.; Sun, X. F.; Cui, J. J.; Gao, B. Y. Interaction between congo red and copper in a binary adsorption system: Spectroscopic and kinetic studies. *Colloids Surf., A* **2009**, *340*, 86−92.
(60) *Malvern, Sample dispersion & refractive index guide*, Version 3.1; 1997; MAN0079.